PCCP

Identification of the Criegee intermediate reaction network in ethylene ozonolysis: Impact on energy conversion strategies and atmospheric chemistry

Journal:	*Physical Chemistry Chemical Physics*
Manuscript ID	CP-ART-01-2019-000473.R1
Article Type:	Paper
Date Submitted by the Author:	25-Feb-2019
Complete List of Authors:	Rousso, Aric; Princeton University Hansen, Nils; Sandia National Laboratories, Combustion Research Facility Jasper, Ahren; Argonne National Laboratory Ju, Yiguang; Princeton University,

Physical Chemistry Chemical Physics

ARTICLE

Identification of the Criegee intermediate reaction network in ethylene ozonolysis: Impact on energy conversion strategies and atmospheric chemistry

Received 00th January 20xx,
Accepted 00th January 20xx

DOI: 10.1039/x0xx00000x

www.rsc.org/

Aric C. Rousso,[a] Nils Hansen,[*b] Ahren W. Jasper,[c] and Yiguang Ju[a]

The reaction network of the simplest Criegee Intermediate (CI) CH_2OO has been studied experimentally during the ozonolysis of ethylene. The results provide valuable information about plasma- and ozone-assisted combustion processes and atmospheric aerosol formation. A network of CI reactions was identified, which can be described best by the sequential addition of CI with ethylene, water, formic acid, and other molecules containing hydroxy, aldehyde, and hydroperoxy functional groups. Species resulting from as many as four sequential CI addition reactions were observed, and these species are highly oxygenated oligomers that are known components of secondary organic aerosols in the atmosphere. Insights into these reaction pathways were obtained from a near-atmsopheric pressure jet-stirred reactor coupled to a high-resolution molecular-beam mass spectrometer. The mass spectrometer employs single-photon ionization with synchrotron-generated, tunable vacuum-ultraviolet radiation to minimize fragmentation via near-threshold ionization and to observe mass-selected photoionization efficiency (PIE) curves. Species identification is supported by comparisons of the mass-selected, experimentally observed photo-ionization thresholds with theoretical calculations for the ionization energies. A variety of multi-functional peroxide species are identified, including hydroxymethyl hydroperoxide ($HOCH_2OOH$), hydroperoxymethyl formate ($HOOCH_2OCHO$), methoxymethyl hydroperoxide (CH_3OCH_2OOH), ethoxymethyl hydroperoxide ($C_2H_5OCH_2OOH$), 2-hydroxyethyl hydroperoxide (HOC_2H_4OOH), dihydroperoxy methane ($HOOCH_2OOH$), and 1-hydroperoxypropan-2-one [$CH_3C(=O)CH_2OOH$]. A semi-quantitative analysis of the signal intensities as function of successive CI additions and temperature provides mechanistic insights and valuable information for future modeling work of the associated energy conversion processes and atmospheric chemistry. This work provides further evidence that the CI is a key intermediate in the formation of oligomeric species via the formation of hydroperoxides.

Introduction

Criegee intermediates (CIs) are carbonyl-oxides that play an important role in the oxidation of unsaturated hydrocarbons with ozone. The dominant chemical pathways for these ozonolysis reactions create primary and secondary ozonides which generate a carbonyl-oxide intermediate, whose importance was first investigated by Rudolf Criegee and now bears his name.[1, 2] The ozonolysis of ethylene, the simplest alkene, involves 1,2,3-trioxolane as the primary ozonide (POZ), 1,2,4-trioxolane as the secondary ozonide (SOZ), and CH_2OO as the CI. In these ozonolysis reactions, the CI is formed vibrationally excited and then can be collisionally stabilized or it will subsequently decompose (into HCO and OH) or isomerize into a 3-membered ring (dioxirane), which further dissociates into H_2O+CO, CO_2+H+H, and H_2+CO_2.

The chemical reactions of CIs are mainly driven by the CI's complex zwitterionic 1,3-bipole character (with a relatively low contribution of the biradical character).[3-5] CIs were found to be important in the atmosphere as intermediates in the ozone-assisted degradation of biogenic hydrocarbons,[6-9] as a contributor to the oxidation of atmospheric NO_x and SO_x,[10-14] and as a source of atmospheric OH and possibly of secondary organic aerosols (SOA).[15-22] For comprehensive description of the CI's reaction pathways we refer the reader to recently compiled reviews.[23, 24]

Early experiments to study the CI reactions were hampered by the CI's short lifetime and low concentrations. Nevertheless, Neeb *et al.* explored the dominant reaction pathways of the CI with water, alcohols, and acids.[25-27] They found that the interactions with water and formic acid especially are many orders of magnitude faster than the initial ozonolysis process, accounting for much of the subsequent hydrocarbon reaction process. Only recently, direct kinetic measurements of CI reactions have become possible through the production of the CI in the laboratory via the CH_2I+O_2 reaction.[28] Subsequently, rates were measured for the reaction of CI with alkenes,[29] acetone, acetaldehyde, and hexafluoroacetone,[30] and H_2O, CH_3CHO, and pollutants such as NO_x and SO_x.[13]

Theoretical calculations have also been employed to explore potential energy surfaces and compute rate constants for many of

[a] Department of Mechanical and Aerospace Engineering, Princeton University, New Jersey 08544, USA.
[b] Combustion Research Facility, Sandia National Laboratories, Livermore, California 94551, USA. Email: nhansen@sandia.gov
[c] Chemical Sciences and Engineering Division, Argonne National Laboratory, Argonne, Illinois 60439, USA.
Electronic Supplementary Information (ESI) available. See DOI: 10.1039/x0xx00000x

these reactions, including those that are difficult to probe experimentally,[29, 31-35] such as the CI self-reaction.[36] While the rate constants derived differ depending on the level of theory and the reaction in question, the overall conclusions are the same: CI reactions are often fast, with low to no activation energy barrier, and CIs readily interact with almost all hydrocarbon species, water, and even ozone, suggesting that an accurate understanding of CI interactions are an important goal for atmospheric chemistry modeling.

Despite these recent successes in exploring chemical rates of individual CI reactions and their impact on atmospheric chemistry, the role of the CI for the formation of secondary organic aerosol (SOA) is still under investigation.[17, 18, 21, 37-39] Recently, Sakamoto *et al.* observed that oligomeric hydroperoxides composed of CH_2OO chain units, formed in the gas-phase, were incorporated into the particle phase following ethylene ozonolysis.[17] They proposed an oligomerization mechanism that is initiated by the reaction of CH_2OO with hydroperoxide species, although they pointed out that knowledge of the hydroperoxides chemistry in the atmosphere is still lacking.

Ozone reactions with hydrocarbons and the subsequent interactions of the CIs have also recently received significant interest in combustion chemistry studies.[40-46] These fundamental investigations are motivated in part by the rise of non-equilibrium plasma-assisted combustion techniques and chemically controlled engine designs such as HCCI (homogenous charge compression ignition). Prerequisites for the development of chemically detailed combustion chemistry models and future engine designs are detailed experimental and theoretical investigations of the reaction network of CIs under combustion-like conditions. As discussed in Ref. [47], and in analogy to atmospheric chemistry, it can be expected that the fast initial ozonolysis reactions generate partially oxidized intermediates, which if not subject to high temperatures, will stabilize and lead to formation of SOAs. However, open questions remain about the initial oxidation mechanism through CI adduct, this importance at intermediate temperatures, and the relative importance of CI interactions with fuel, intermediate, and product species.

To expand our knowledge of the CI reaction network at over a relevant temperature range, we investigated ethylene ozonolysis in laboratory experiments between 300 and 1000 K using a jet-stirred reactor at near-atmospheric pressure with molecular-beam mass spectrometry. In a previous paper,[46] which focused on the main ethylene ozonolysis pathways and primary product species, we described the detection and identification of the key intermediates such as hydroperoxy-acetaldehyde ($HOOCH_2CHO$, the keto-hydroperoxide in ethylene ozonolysis) in the low-temperature oxidation resulting from ozone-assisted oxidation of ethylene below 600 K. Significant production was observed of oxygenated intermediates, such as formaldehyde (CH_2O), methanol (CH_3OH) and ethanol (CH_3CH_2OH), acetaldehyde (CH_3CHO), hydroxy-acetaldehyde ($HOCH_2CHO$), hydrogen peroxide (H_2O_2), methyl hydroperoxide (CH_3OOH), ethyl hydroperoxide (CH_3CH_2OOH), formic acid (HCOOH), as well as primary products such as H_2O, CO and CO_2. The formation routes of many of these intermediates are not entirely clear at this point, however the knowledge about their presence is sufficient for the detailed analysis presented here. Due to the thermal decomposition of O_3, ozone-initiated reactions were observed to cease at temperatures above ~600 K. Smaller concentrations of other oxygenated species were found within the mass spectrum, suggesting the need for further study and understanding of the CI interactions present.

In this paper, we report the detection and identification of the complex CI reaction network under these idealized laboratory conditions. Specifically, we observe eleven individual reaction sequences in which the CI appears to be sequentially inserted into the intermediate species forming oligomeric hydroperoxides. Oligomerization via CI reaction sequences starting from C_2H_4, water, formic acid, alcohols, hydroperoxides, aldehydes, and the bifunctional hydroxy-acetaldehyde and hydroperoxy-acetaldehyde were identified in the mass spectra. The products of up to four sequential CI insertion steps were observed, resulting in highly oxygenated oligomeric hydroperoxide species. As described above, the observed highly oxygenated intermediates are possibly important for the formation of tropospheric SOAs.[17, 20, 48-50] Calculated ionization energies of the first-step intermediates are consistent with the experimentally observed ionization thresholds. The experimental observations are best described as 1,3-cycloadditions reactions of the CI with C=C and C=O double bonds and as insertion reactions into acidic -OH and -OOH groups.

The results presented here help to elucidate the formation pathways of the oligomers and the importance of them on SOA formation and plasma-assisted combustion processes. While our results are interpreted here to extract qualitative mechanistic insights into this CI reaction network, these data also provide targets for future quantitative chemical modeling studies to validate detailed atmospheric and ozone-assisted combustion mechanisms.

Experimental and theoretical approaches

Experimental apparatus and procedures

The ozonolysis of ethylene was studied using the Sandia jet-stirred reactor (JSR) that is coupled to a molecular-beam mass spectrometer employing photoionization via synchrotron-generated vacuum-ultraviolet (VUV) radiation.[51, 52] The experimental details and procedures were identical to the experiments described in Ref. [46] and are not repeated here extensively. In short, the JSR is a 33.5 cm^3 fused silica sphere with four injector nozzles located near the center of the JSR. Gas flows through these nozzles (with an inner diameter of ~1 mm) created stirring gas jets which resulted in a homogenous – both in temperature and species composition – mixture within the JSR for analysis of steady state processes. Upstream of the reactor itself, calibrated MKS mass flow controllers were used to regulate concentric O_2/O_3 and ethylene streams, both diluted by argon, which mix just prior to entering the injectors.

The entire assembly was housed in a stainless-steel pressure vessel with water cooling. Temperatures were measured by thermocouple (K-Type, Thermocoax) just outside the reactor and at the sampling location. The exhaust gases were removed continuously for constant temperature and pressure operation. For ozone production, a fraction of the oxidizer stream was fed through an ozone generator (Oriel) and a 70-cm quartz absorption cell prior to the JSR assembly. A helium-neon UV calibration lamp was used

along with an Ocean Optics spectrometer for O_3 concentration measurements at 312.57 nm. Using the known ozone absorption cross-sections,[53] the ozone concentration as a function of oxygen flow rates through the generator was calibrated and continuously monitored during our experiments.

By enclosing the reactor in an oven and performing experiments through a range of temperatures, the temperature dependence of species concentrations was measured, which allows for chemical insights and 0-D modeling of the underlying chemical reaction pathways. In this experiment, the reactor was operated from 300-1000 K, at a constant pressure of 700 Torr. A nominal residence time of τ = 1.3 s, stoichiometry of φ = 0.5 with 86% argon dilution (2% ethylene, 12% O_2, 86% Ar mole fraction) and ozone concentration of 1000 ppm was maintained for all experimental conditions. Gas mixture flow rates were adjusted to maintain this residence time with increasing temperature for all cases, and pre-corrected to account for temperature shift from the probe from previous studies.[51, 52, 54, 55]

At the exit to the JSR, the reaction intermediates and products were sampled through a quartz nozzle with a 40° cone angle and a ~50 μm tip diameter into a custom, time-of-flight, reflectron molecular beam mass spectrometer.[51, 52, 56, 57] The MBMS has a sensitivity of ~1 ppm, a large dynamic range, and a mass resolution of $m/\Delta m$ ~4000. Photo-ionization of the molecular beam occurs through crossing of a synchrotron-generated VUV photon beam (10^{14} photons/s) at Terminal 3 of the Chemical Dynamics Beamline of the Advanced Light Source at Lawrence Berkeley National Laboratory (LBNL). The photon beam has high tunability and a resolution of E/ΔE (fwhm) ~250-400 in the region from 7.4 to 30 eV for isomer specificity and near threshold ionization to reduce fragmentation.[58]

To obtain quantitative insights, mass spectra covering the temperature range from 300-1000 K were taken at photon energies of 9.5, 10.0, 10.5, 11.0, 12.3, 14.35, 16.2 and 16.65 eV. Using routines described previously,[52, 59] this extensive set of photon energies has been proven to be useful for converting the respective mass spectra into temperature-dependent concentration profiles because it enables near threshold ionization measurements of species concentration.

A typical mass spectrum from *m/z* = 50 to 180 is shown in Fig. 1. This mass spectrum was obtained at 333 K and a photon energy of 11.0 eV. Groups of peaks containing 4 to 11 heavy atoms (carbon and oxygen atoms) are marked. The grouped species are generally highly oxygenized, containing up to 7 oxygen atoms.

For the analysis of the complex reaction network of the CI, a high-resolution mass spectrometer is indispensable. It is shown in Fig. 2 that in this experiment, the resolution is sufficient to distinguish between species of the same nominal mass but different numbers of C and O atoms. Shown are the peaks of the nominal masses at 74, 92, and 138, which, based on their flight time, were identified as $C_2H_2O_3$ (*m/z* = 74.000) + $C_3H_6O_2$ (74.037), $C_2H_4O_4$ (92.011) + $C_3H_8O_3$ (92.047), and $C_2H_2O_7$ (137.980) + $C_3H_6O_6$ (138.016) + $C_4H_{10}O_5$ (138.053). While it is discussed in this paper that most of these peaks can be attributed to insertion reactions of the CI (CH_2OO), the identity or origin of the observed $C_2H_2O_7$ is not obvious and shall not be further explored here.

To help with the identification of multiple repetitive reaction sequences, mass-selective PIE curves were recorded through

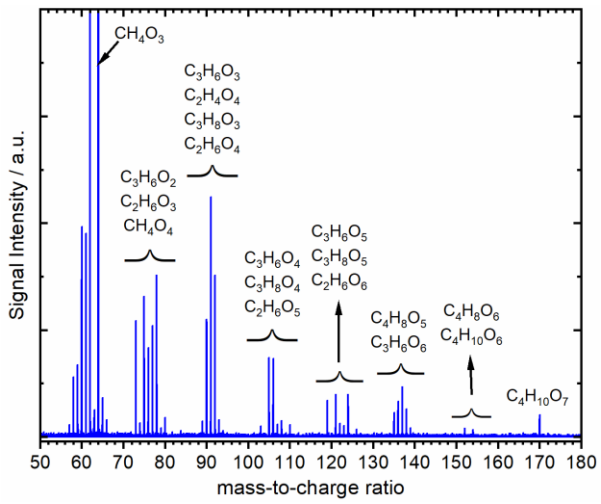

Figure 1: Typical JSR-sampled mass spectrum obtained from the ethylene ozonolysis reaction network at 333 K.

scanning of the photon energy from 9.0 to 11.0 eV in 0.05 eV steps at a constant reactor temperature. This step size has been proven sufficient for many species identification studies as it is near the above-mentioned width of the energy distribution of the ionizing photons and the accuracy of the theoretical calculations as described below.[60-62] The observed ionization thresholds were compared with theoretical calculations of ionization energies of the initial CI addition product. It should be kept in mind, that, although this combination of theory and experiment has been proven to be exceptionally powerful for isomeric identification and quantification in reactive systems, limitations are reached for molecules containing more than seven heavy atoms.[56, 57] More details will be provided in the "Species identification" section.

Beyond identification of the intermediates, their quantification is an important step to provide targets for model development and validation. To convert these mass spectra into absolute mole fractions of the individual species, previously developed routines are applied,[52] which are based on the fact that the signal count *S* at a given *m/z* ratio and photoionization energy is related to the mole fraction x_i using the following equation:

$$S_i(E,T) = x_i(T) \times \varphi(E) \times \mathrm{SW} \times D(M_i) \times c \times \mathrm{FKT}(T) \times \sigma_i(E) \quad \text{(E1)}$$

Where $\varphi(E)$ is the number of photons (measured using a calibrated photodiode), SW is the number of scans, $D(M_i)$ is the mass discrimination factor for species *i*, and c is an instrument factor. FKT is a sampling function dependent on the temperature, which can be determined (as c×FKT) assuming the concentration of argon is known. $\sigma_i(E)$ is the absolute photoionization cross section, which is both molecule and energy dependent.

Unfortunately, the exact photoionization cross sections for the species studied here are unknown, as they are often not stable enough for known concentrations to be experimentally measurable. Earlier theoretical work has shown that for hydroperoxide species, which are in the focus of this work, the cross section is in the order of ~7 Mb at 0.5 eV above the ionization threshold.[52] However, considering that the species in question have upwards of 5 or 6 heavy atoms, we expect the uncertainty of the theoretically calculated

photoionization cross sections to be very large and therefore of questionable usefulness.

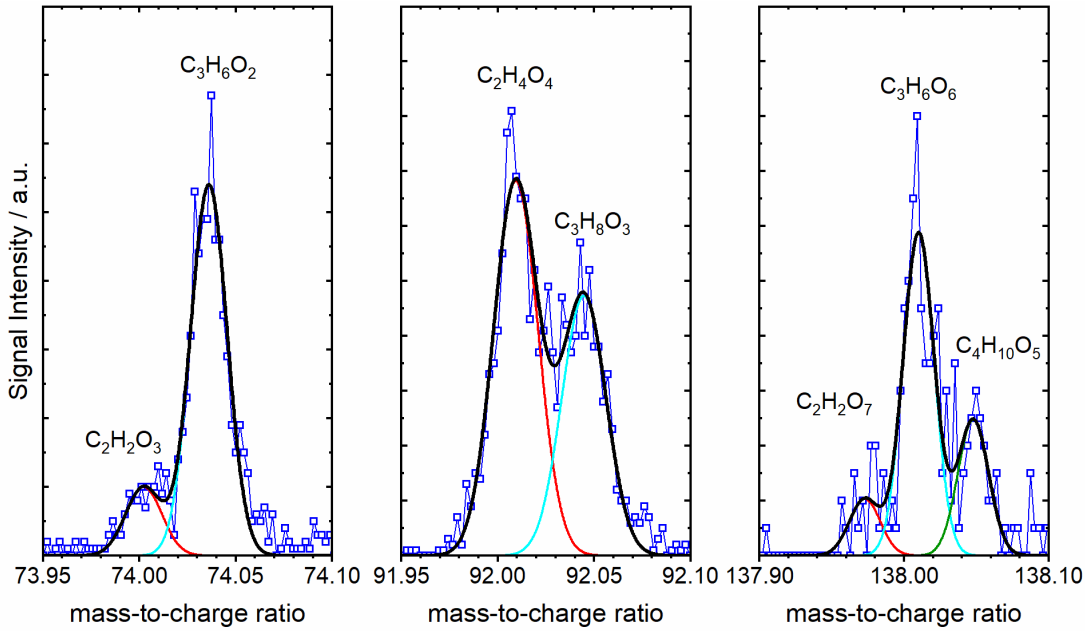

Figure 2: High-resolution mass spectrum of ethylene ozonolysis in a JSR. The mass spectra reveal the presence of highly oxygenated species. Left: Signal related to $C_2H_2O_3$ and $C_3H_6O_2$. Middle: Detection of $C_2H_4O_4$ and $C_3H_8O_3$. Right: Peaks at the nominal *m/z* ratio of 138 are assigned to $C_2H_2O_7$, $C_3H_6O_6$, and $C_4H_{10}O_5$.

Instead, we report here only the $x_i(T) \times \sigma_i(E)$ product. Once an accurate $\sigma_i(E)$ becomes available, the results can instantaneously be converted into mole fraction profiles. The $x_i(T) \times \sigma_i(E)$ product is conservatively estimated to be good within ±20% due to cumulative uncertainties in photodiode measurement, mass discrimination factor, and argon concentration. Because it is expected that all cross sections fall within the same order of magnitude, these reported weighted "mole fractions" can still be used to judge relative production with respect to each other. Absolute concentrations are also not important to support our conclusions on species formation pathways and relative reaction rates.

Species identification

As demonstrated previously, calculated ionization energies and experimentally measured photo-ionization energy (PIE) curves, when available, can provide unambiguous structural assignments at specific *m/z* ratios.[57, 60, 62, 63] This approach was used successfully to study reactive mixtures,[56, 57, 64, 65] but it is increasingly difficult to apply to large species with lengthy chains, such as the adducts of interest here that are formed via successive CI additions. Here we limit our most detailed ionization energy calculations to species formed via the first CI addition step of the various CI addition sequences. Selected PIE curves for intermediates formed from two sequential addition reactions are shown in the Supplemental Material.

In this work (for only the first addition reaction), several isomers were considered for each *m/z*, but a comprehensive study of all conceivable isomers and definitive assignments was not pursued. Instead, ionization energies of certain isomers based on proposed chemical pathways were calculated, and these results are used to confirm the consistency of the proposed chemistry with the experimentally observed ionization thresholds.

Isomer assignments based on observed ionization thresholds are particularly difficult for large linear systems due to increased fragmentation and multiple low-lying conformers with broad Franck–Condon overlaps and widely varying "local" ionization energies, as discussed in Moshammer *et al.*[51] Due to these complications, experimental ionization thresholds are typically much less sharp for large species than for small species and can in fact extend over many tenths of an eV. It is therefore often difficult to determine precise ionization energies, both experimentally and theoretically and to distinguish between isomers with broad overlapping threshold regions.[56, 57] Coupled with low concentrations and weak PIE signals, the unambiguous assignment of some of the larger molecular structures in the present experiments was not always possible. Nevertheless, this procedure, along with a priori chemical knowledge of the possible chemical pathways, allows for some discrimination of competing mechanisms even when definitive assignments are not possible.

To address some of the computational challenges described above, an automated strategy has been implemented to systematically explore conformeric structures and to compute up to ~$N_{torsion}^3$ locally adiabatic ionization energies[51] for the systems of interest here, where $N_{torsion}$ is the number of rotatable bonds. The cheminformatics tool, Open Babel,[66, 67] was used to generate initial geometry guesses from the chemical structure. Candidate conformers were then generated by spinning all rotatable bonds by fixed step sizes. A step size of 120° was used for torsions with sp^3 hybridization for both central atoms (the majority of cases), and 60° step sizes were used otherwise (e.g., for torsions where one of the

rotatable groups is the –CHO group). Each candidate structure was minimized first using Open Babel's automated conformer generating strategy "confab" and then using M06-2X/cc-pVDZ. The structures were checked for duplicates, including mirror images, and higher-level ionization energies were computed for the unique conformers using the ~CCSD(T)/CBS//M06-2X/cc-pVTZ level of theory, where ~CCSD(T)/CBS indicates that the complete basis set limit correction to CCSD(T)/cc-pVTZ was estimated using MP2 and the cc-pVTZ and cc-pVQZ basis sets, as employed elsewhere.[46, 51] The locally adiabatic ionization energy was computed for each conformer. Often, the locally adiabatic ionization energies are in close agreement with one another and with the global adiabatic ionization energy, and unless otherwise indicated the values given below are the locally adiabatic ionization energy for the lowest-energy conformer. The consideration of higher-energy conformers is sometimes useful for interpreting the observed PIE curves, as noted below. As discussed and demonstrated in previous publications,[56, 57, 60-62] calculated adiabatic ionization energies are often good predictors of the experimental ionization thresholds and are thus typically sufficient for species identification. Occasionally, poor Franck-Condon overlaps between the ground-state and ionized species can preclude a sensitive detection of the ionization threshold and thus complicate these assignments. This complication will be noted below when it is suspected.

An uncertainty of ±0.1 eV is assigned to the calculated ionization energies as indicated in the respective figures as gray boxes.

Results and discussion

The mass spectra obtained via ozonolysis of ethylene can be largely interpreted as the result of consecutive additions of CI to typical small-molecule combustion intermediates and products. Together with evidence presented in the literature,[17, 26] the results discussed here suggest that such oligomerization reaction sequences can lead to highly oxygenated adducts. An example is shown in Fig. 3 for the sequential CI addition starting from methanol (CH_3OH), leading eventually to $C_4H_{10}O_7$, possibly via three CI additions:

$$CH_3OH + CH_2OO \rightleftarrows HOOCH_2OCH_3 \quad (R1)$$

$$HOOCH_2OCH_3 + CH_2OO \rightleftarrows H(OOCH_2)_2OCH_3 \quad (R2)$$

$$H(OOCH_2)_2OCH_3 + CH_2OO \rightleftarrows H(OOCH_2)_3OCH_3 \quad (R3)$$

Although it is discussed further below that the molecular structures of the reaction products of R1-R3 cannot be unambiguously assigned, the repetitive features of the mass spectra support the interpretation of sequential addition reactions driven by the insertion and addition of CIs.

Ethylene, water, and several alcohols, hydroperoxides, aldehydes, and acids are identified in this work as the base molecules for multiple CI addition reactions. In addition, multi-functional molecules containing aldehyde and -OH or -OOH functional groups can act as starting molecules for CI insertion reactions.

In this Section, evidence for this CI oligomerization reaction network is provided first via the repetitive nature of the mass spectra and the consistency between the experimentally observed photoionization thresholds and the theoretically calculated values for the initial intermediate of the individual addition sequence. An attempt to identify the chemical structures of the products of the second, third, and fourth addition of a Criegee Intermediate was not made. The reasons, aside from the difficulty in computation discussed above, are mostly due to the insufficient signal-to-noise ratio for the heavy intermediates, the large number of conceivable

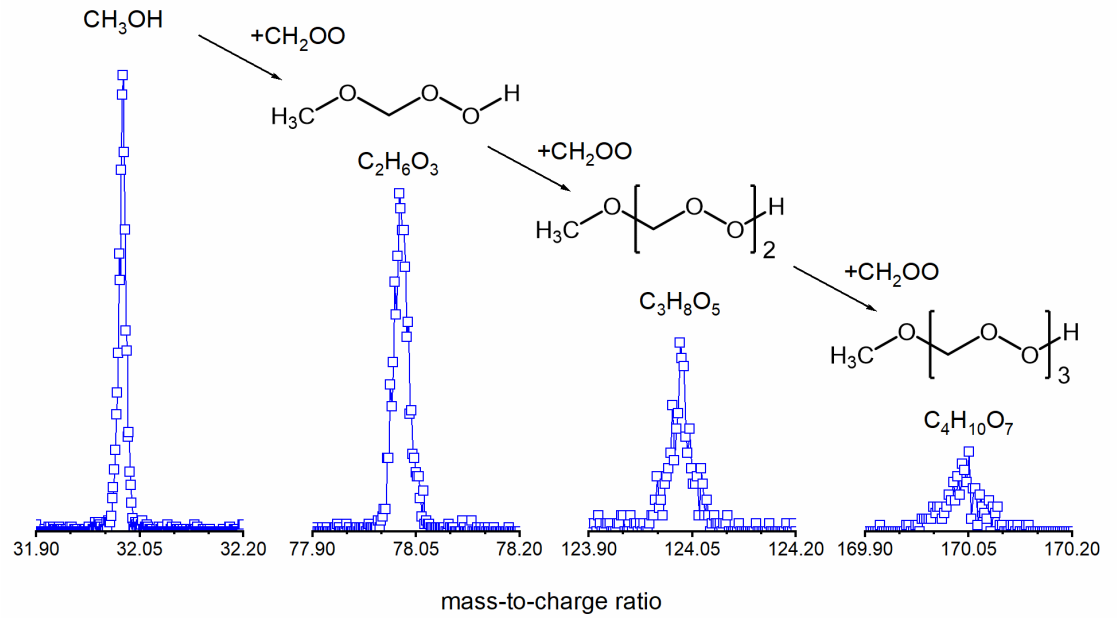

Figure 3: Identification of sequential addition CI addition reactions in the JSR-sampled mass spectra following ethylene ozonolysis. Although other isomeric structures are conceivable beyond the ones indicated, these addition reactions lead to highly oxygenated oligomeric peroxides with the CI as the chain unit. See text for details.

isomers which makes an isomeric identification unfeasible, and theoretical efforts that become too demanding.[57] Nevertheless, the presented interpretation of the mass spectra with a focus on possible formation pathways of the oligomeric highly oxygenated molecules seem plausible and consistent with the literature. To guide the discussion, Table 1 summarizes the intermediates that were detected in this work together with their names as used in this contribution, and conceivable molecular structures and calculated and observed ionization thresholds.

Furthermore, this Section contains a critical assessment of the observed signal intensities and provides further mechanistic insights with respect to SOA formation. The temperature dependencies of the mole fraction profiles of these intermediates are also discussed.

Reaction of the CI with ethylene and subsequent addition reactions

Evidence for the addition of a CI to an olefin was first reported by Story and Burgess.[68] Such reactions belong to the class of 1,3-dipolar

Parent Species	#	Name of the CI Adduct as used in this paper	*m/z*	Chemical Formula	Conceivable CI Adduct Structure	Calc. IE	Exp. IE	Possible *Reactants* (+ CH_2OO)
C_2H_4	1	3-hydroxypropanal (3HP) allyl hydroperoxide (AHP)	74.037	$C_3H_6O_2$	$HOCH_2CH_2CHO$ $C_2H_3CH_2OOH$	9.87 9.59	9.90 9.55	C_2H_4
	2		120.042	$C_4H_8O_4$	$C_3H_5OOCH_2OOH$ $HOOCH_2OCH_2CH_2CHO$		9.55 9.55	$C_2H_3CH_2OOH$ $HOCH_2CH_2CHO$
	3		166.048	$C_5H_{10}O_6$	$C_3H_5OO(CH_2OO)_2H$ $H(OOCH_2)_2OCH_2CH_2CHO$			$C_3H_5OOCH_2OOH$ $HOOCH_2OCH_2CH_2CHO$
	4		212.053	$C_6H_{12}O_8$	$C_3H_5OO(CH_2OO)_3H$ $H(OOCH_2)_3OCH_2CH_2CHO$			$C_3H_5OO(CH_2OO)_2H$ $H(OOCH_2)_2OCH_2CH_2CHO$
H_2O	1	hydroxymethyl hydroperoxide (HMHP)	64.016	CH_4O_3	$HOOCH_2OH$	9.83	9.85	H_2O
	2		110.022	$C_2H_6O_5$	$HOOCH_2OCH_2OOH$ $HOCH_2OOCH_2OOH$		10.05	$HOOCH_2OH$
HCOOH	1	hydroperoxymethyl formate (HPMF)	92.011	$C_2H_4O_4$	$HOOCH_2OCHO$			HCOOH
CH_3OH	1	methoxymethyl hydroperoxide (MMHP) 2-hydroxyethyl hydroperoxide (HEHP)	78.032	$C_2H_6O_3$	$HOOCH_2OCH_3$ $HOCH_2CH_2OOH$	9.56 9.71	9.58 9.70	CH_3OH $HOCH_2CH_2OO + HO_2$
	2		124.037	$C_3H_8O_5$	$H(OOCH_2)_2OCH_3$		9.75	$HOOCH_2OCH_3$
	3		170.043	$C_4H_{10}O_7$	$H(OOCH_2)_3OCH_3$			$H(OOCH_2)_2OCH_3$
	4		216.048	$C_5H_{12}O_9$	$H(OOCH_2)_4OCH_3$			$H(OOCH_2)_3OCH_3$
C_2H_5OH	1	ethoxymethyl hydroperoxide	92.047	$C_3H_8O_3$	$HOOCH_2OCH_2CH_3$	9.44	9.47	CH_3CH_2OH
	2		138.053	$C_4H_{10}O_5$	$HOOCH_2OOCH_2OCH_2CH_3$			$HOOCH_2OCH_2CH_3$
CH_3CHO	1	1-hydroperoxypropan-2-one	90.032	$C_3H_6O_3$	$CH_3C(=O)CH_2OOH$	9.57	9.62	CH_3CHO
	2		136.037	$C_4H_8O_5$			9.50	
	3		182.043	$C_5H_{10}O_7$				
H_2O_2	1	dihydroperoxy methane (DHPM)	80.011	CH_4O_4	$HOOCH_2OOH$	9.89	9.85	H_2O_2
	2		126.016	$C_2H_6O_6$	$HOO(CH_2OO)_2H$			$HOOCH_2OO$
	3		172.022	$C_3H_8O_8$	$HOO(CH_2OO)_3H$			$HOO(CH_2OO)_2H$
CH_3OOH	1		94.027	$C_2H_6O_4$	$CH_3O(-O)CH_2OOH$	9.72	9.77	CH_3OOH
	1				$HOCH_2OCH_2OOH$	9.66		
C_2H_5OOH	1		108.042	$C_3H_8O_4$	$C_2H_5(-O)CH_2OOH$ $HOC_2H_4OCH_2OOH$	9.55 9.57	9.52	C_2H_5OOH
	2		154.048	$C_4H_{10}O_6$				
	3		200.053	$C_5H_{12}O_8$				
$HOCH_2CHO$	1		106.027	$C_3H_6O_4$	$HC(=O)OCH(OH)CH_2OH$ $HOCH_2C(=O)OCH_2OH$	9.83 9.99	9.93	$HOCH_2CHO$
	2		152.032	$C_4H_8O_6$				
$HOOCH_2CHO$	1		122.022	$C_3H_6O_5$			9.93	$HOOCH_2CHO$
	2		168.027	$C_4H_8O_7$				
	3		214.032	$C_5H_{10}O_9$				

Table 1: List of detected intermediate structures, identified intermediates, and their conceivable structures and reaction pathways.

cycloaddition in which a five-membered transition state is formed. Because of the 1,3-bipolar structure of the CI, which is similar to the zwitterionic structure of ozone, the reaction of ethylene with the CI can be expected to be similar to the ozonolysis reaction.[36, 69] Crehuet *et al.*[69] and Lan *et al.*[70] have shown that the CI addition reactions have lower barriers than the analogous ozonolysis reactions. According to Vereecken *et al.*,[36] the olefin + CI reaction leads to a cyclic peroxide (*cycl.*-$CH_2CH_2CH_2OO$-), which is significantly more stable than the corresponding primary ozonide (POZ, 1,2,3-trioxolane) formed in the ozonolysis. The reaction of the CI (CH_2OO) with ethylene was studied by Buras *et al.*,[29] who provided experimental and theoretically predicted rate coefficients for the C_2H_4 + CH_2OO reaction. While rate constants were measured by observing the consumption of the CI, the identification of the product channels was not attempted in their work.

The JSR-sampled mass spectra contain a peak at *m/z* = 74.037 ($C_3H_6O_2$) that points towards a reaction of C_2H_4 with the CI. The corresponding PIE curve at 400 K is shown in Fig. 4, exhibiting an ionization threshold near 9.55 (± 0.05) eV and a sharper rise near 9.90 (± 0.05) eV. While the first threshold is close to the detection limit, indicating only a small concentration of the respective intermediate, the second threshold near 9.90 eV is clearly visible.

According to previous work,[36] the direct CH_2OO addition to ethylene results in a ring formation to 1,2-dioxolane (*cycl.*-$CH_2CH_2CH_2OO$-). However, the calculated ionization energy of this isomer is 9.09 eV and does not match the experimentally observed threshold. Significant formation of this cyclic product under our conditions can therefore be excluded.

It was shown by Pfeifle *et al.* that the primary ozonide can undergo ring opening via a diradical structure to form a keto-hydroperoxide,[71] an analogous reaction seems conceivable for the 1,2-dioxolane as well, resulting in 3-hydroxypropanal (3HP, $HOCH_2CH_2CHO$). Our calculated ionization energy for 3HP is 9.87 eV, which matches the higher-energy feature around 9.90 eV seen in Fig. 4.

The decomposition of 1,2-dioxolane to form allyl hydroperoxide (AHP, CH_2CHCH_2OOH) was also considered. Olefenic hydroperoxides, molecules with a C=C double bond and a hydroperoxide group, have been quite elusive and only recently such compounds were identified as important intermediates in low-temperature oxidation chemistry of hydrocarbons.[72-74] Nine conformers of allyl hydroperoxide were included in the ionization energy calculation, and the adiabatic ionization energy was determined to be 9.59 eV. This IE corresponds well with the experimental threshold observed at 9.55 eV. Overall, the experimental data is consistent with the presence of AHP, with contributions from 3HP that cannot be ruled out.

Beyond the first adduct at *m/z* = 74.037 ($C_3H_6O_2$), additional reaction intermediates from sequential additions of the CI have been detected at *m/z* = 120.042 ($C_4H_8O_4$), 166.048 ($C_5H_{10}O_6$), and 212.053 ($C_6H_{12}O_8$). With the experimental data being consistent with the first intermediate of the CI addition sequence being the olefinic allyl hydroperoxide and/or the 3-hydroxypropanal, the observed reaction sequence(s) can then be described best as formation of oligomeric hydroperoxides through addition to the hydroxy or hydroperoxy group or the aldehyde function:

$$C_2H_4 + CH_2OO \rightleftarrows C_2H_3CH_2OOH \quad (R4)$$

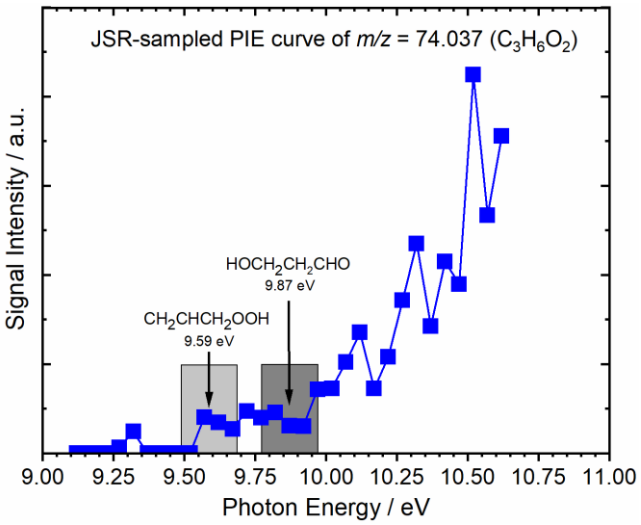

Figure 4: The observed JSR-sampled photoionization efficiency curve of *m/z* = 74.037 ($C_3H_6O_2$) after ethylene ozonolysis is consistent with the calculated ionization energies of olefinic allylhydroperoxide (CH_2CHCH_2OOH) and 3-hydroxypropanal ($HOCH_2CH_2CHO$).

$$C_2H_3CH_2OOH + CH_2OO \rightleftarrows C_3H_5OOCH_2OOH \quad (R5)$$

$$C_3H_5OOCH_2OOH + CH_2OO \rightleftarrows C_3H_5OO(CH_2OO)_2H \quad (R6)$$

$$C_3H_5OO(CH_2OO)_2H + CH_2OO \rightleftarrows C_3H_5OO(CH_2OO)_3H \quad (R7)$$

$$C_2H_4 + CH_2OO \rightleftarrows HOCH_2CH_2CHO \quad (R8)$$

$$HOCH_2CH_2CHO + CH_2OO \rightleftarrows HOOCH_2OCH_2CH_2CHO \quad (R9)$$

$$HOOCH_2OCH_2CH_2CHO + CH_2OO \rightleftarrows H(OOCH_2)_2OCH_2CH_2CHO \quad (R10)$$

$$H(OOCH_2)_2OCH_2CH_2CHO + CH_2OO \rightleftarrows H(OOCH_2)_3OCH_2CH_2CHO \quad (R11)$$

Allyl hydroperoxide can also react with the CI via a 1,3-dipolar cycloaddition to the C=C double bond leading to five-membered di-oxolane-type ring structures which can undergo ring-opening to form complex $C_4H_8O_4$ isomers. Reactions of the CIs with the -OOH and -OH functionalities are discussed further below. The feasibility of such insertion reactions and their role towards the formation of the oligomeric hydroperoxides in SOA have also been discussed in the literature.[17, 75, 76] Reactions of the CI with the aldehyde function (as in 3HP) are likely to proceed via a secondary ozonide and will be discussed further below.

For reasons described above, a definitive identification of the isomeric compositions of the heavy reaction products of reactions R5-R7 and R9-R11 was not attempted here. Instead, we note that within this series, species concentrations decrease with increasing number of CH_2OO additions. A more detailed analysis of the signal intensities is provided at the end of the "Results and discussion" section.

Reaction of the CI with water and subsequent addition reactions

The formation of oligomeric hydroperoxides with the CI as the chain unit were also observed starting from the interactions of the CI with water. It has been previously reported that the CI can react with water to form hydroxymethyl hydroperoxide (HMHP):[15, 27, 33, 77, 78]

$$CH_2OO + H_2O \rightleftarrows HOCH_2OOH \qquad (R12)$$

The PIE curve for CH_4O_3 (*m/z* = 64.016) at 400 K is shown in Fig. 5.

The main contribution to the signal matches very well with the previous data from Moshammer *et al.,*[51] who observed a strong peak at CH_4O_3 in the low-temperature oxidation of dimethyl ether and assigned it to a fragment from dissociative ionization of the ketohydroperoxide hydroperoxymethyl formate (HPMF, $HOOCH_2OCHO$). It is discussed in the next Section that in this study, HPMF is likely to be the product of the well-known reaction of the CI with formic acid. Therefore, the main feature of the PIE curve of Fig. 5 suggests that CH_4O_3 is a fragment of the HPMF cation ($HOOCH_2OCHO^+ \rightarrow HOOCH_2OH^+ + CO$), at a calculated fragment appearance energy of AE = 10.07 eV,[51] which matches the observed appearance energy of 10.05 eV.

However, the inset in Fig. 5 reveals an additional feature in the ethylene ozonolysis experiments. Based on the excellent match between the experimentally observed and calculated ionization energy for the hydroxymethyl hydroperoxide ($HOCH_2OOH$, HMHP), this additional feature in the PIE curve is consistent with the presence of the bifunctional HMHP which most likely results from reaction R12.

Lin *et al.* used *ab initio* methods to calculate the potential energy of reaction R12.[79] Based on their methods, a barrier of ~3 kcal/mol was determined which may indicate the limited importance compared to other CI reactions, which typically have submerged barriers. However, there is sufficient uncertainty in these calculations that lower barriers and fast atmospheric-temperature rates cannot be ruled out. The HMHP from reaction R12 is the starting point for an additional CI insertion reaction leading to an intermediate at *m/z* = 110.022 ($C_2H_6O_5$). It is not known whether the CI inserts into the OH of the hydroxy or hydroperoxy group of the HMHP and thus two different reaction products are conceivable:

$$HOCH_2OOH + CH_2OO \rightleftarrows HOCH_2OOCH_2OOH \qquad (R13)$$

$$HOCH_2OOH + CH_2OO \rightleftarrows HOOCH_2OCH_2OOH \qquad (R14)$$

An attempt to identify the structure of the $C_2H_6O_5$ intermediate was not made. However, given the rate expressions for reactions of alcohols and hydroperoxides with the CI,[75, 76] reactions of the alcohol functions are more likely, thus the formation of the dihydroperoxide ether $HOOCH_2OCH_2OOH$ (reaction R14) should be preferred over R13. In principle, oligomerization can continue via the reaction of $HOOCH_2OCH_2OOH$ and/or $HOCH_2OOCH_2OOH$ with CI, but the products of such addition reactions were not detected under the current experimental conditions. This is likely due to species concentrations decreasing and signal intensities dropping below our detection threshold. This trend is discussed in more detail at the end of the "Results and discussion" section.

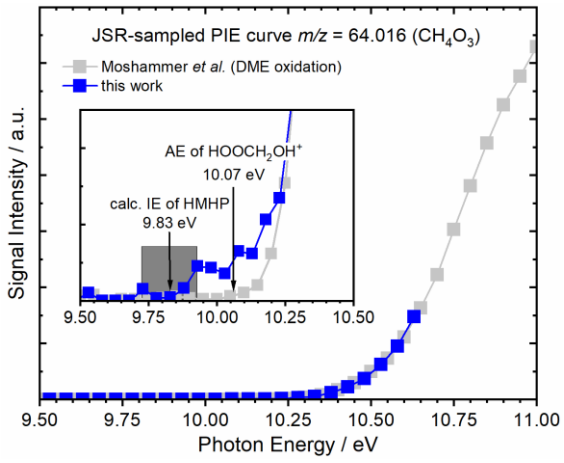

Figure 5: JSR-sampled PIE curve of *m/z* = 64.016 (CH_4O_3) during ethylene ozonolysis. The main feature can be identified as a fragment of hydroperoxymethyl formate (HPMF), and the additional feature starting at 9.85 eV is due to the presence of hydroxymethyl hydroperoxide (HMHP). The inset shows the curve near threshold magnified by 150x. See text for details.

Reaction of the CI with formic acid: Formation of hydroperoxymethyl formate (HPMF) and subsequent addition reactionsand subsequent addition reactions

A third reaction sequence starts from the reaction of the CI with formic acid. The first step of this reaction is well known to lead to the hydroperoxymethyl formate (HPMF, $HOOCH_2OCHO$):[25-27]

$$CH_2OO + HCOOH \rightleftarrows HOOCH_2OCHO \qquad (R15)$$

Formic acid has been shown in our previous work and in the literature to be present in ethylene ozonolysis and its formation is well understood.[25, 27, 46] Significant HPMF formation is seen in the ethylene ozonolysis system, along with subsequent CI adducts. The identity of the HPMF is tentatively confirmed through the observation of the corresponding CH_4O_3 fragment at *m/z* = 64.016 (see Fig. 5). The detailed analysis of this PIE curve at *m/z* = 92.011 ($C_2H_4O_4$) and associated isomeric formation, however, will be the subject of future work, as it directly ties into key aerosol formation in atmospheric measurements. In the interest of completeness for the ethylene reaction system in this work, however, it is clearly present and follows previous experimental results which confirms its identity and importance.

Reaction of the CI with alcohols and subsequent addition reactions

Our previous results[46] indicated significant formation of methanol (CH_3OH) and ethanol (C_2H_5OH) in the ozone-assisted oxidation of ethylene in the low-temperature regime and it is now understood that the CI can insert itself in the OH alcohol function.[35, 76] Consecutive addition reactions of the CI with methanol and ethanol were observed in this study.

Methanol is a known scavenger for the CI, that is, the reactions of CH_3OH and the CI are very fast. The kinetics of alcohol+CI reactions

have been studied theoretically and experimentally by Tadayon *et al.*[76] Based on their results, the methanol/ethanol+CI reactions should lead to alkoxymethyl hydroperoxides: methoxymethyl hydroperoxide (MMHP, $HOOCH_2OCH_3$ at *m/z* = 78.032) and ethoxymethyl hydroperoxide (EMHP, $C_2H_5OCH_2OOH$ at *m/z* = 92.047) as the products. The CI addition to CH_3OH and C_2H_5OH should form MMHP and EMHP through reactions R1 and R16:

$$C_2H_5OH + CH_2OO \rightleftarrows C_2H_5OCH_2OOH \quad (R16)$$

The measured PIE curve for the *m/z* = 78.032 ($C_2H_6O_3$) intermediate in the ozonolysis experiments is shown in Fig. 6. The observed onset of 9.58 (±0.05) eV is consistent with the calculated values for the MMHP. For this intermediate, 13 different conformeric structures were considered, with the adiabatic IE at 9.56 eV.

Another possible $C_2H_6O_3$ isomer at *m/z* = 78.032 is 2-hydroxyethyl hydroperoxide (HEHP, $HOCH_2CH_2OOH$), suggested by Sakamoto *et al.*[17] to be formed through the reaction scheme with OH:

$$C_2H_4 + OH \rightleftarrows HOCH_2CH_2 \quad (R17)$$

$$HOCH_2CH_2 + O_2 \rightleftarrows HOCH_2CH_2OO \quad (R18)$$

$$HOCH_2CH_2OO + HO_2 \rightleftarrows HOCH_2CH_2OOH + O_2 \quad (R19)$$

The calculated ionization energy for the HEHP isomer of 9.71 eV is also marked in Fig. 6. As can be seen, this calculated value falls together with an experimentally observed onset near 9.7 eV. The theoretical calculations showed that locally adiabatic IEs for the low-lying conformeric states are near 9.65 eV which would agree with the experimental observations.

Based on this analysis, the isomeric identities of the *m/z* = 78.032 cannot be unambiguously unraveled. The experimental results are consistent with the presence of the MMHP, but contributions from the HEHP cannot be excluded.

For $C_3H_8O_3$, the observed ionization threshold agrees with the calculated ionization energy of the isomeric structure of $HOOCH_2OCH_2CH_3$ ($C_3H_8O_3$) as shown in Fig. 6. For this intermediate, a total of 38 conformer structures were considered with locally adiabatic ionization energies ranging from 9.14 to 9.9 eV. The lowest energy conformer has an IE of 9.44 eV, which matches well with the observed experimental rise at 9.47 (±0.05) eV.

Products of additional insertion reactions were detected at *m/z* = 124.037 ($C_3H_8O_5$), 170.043 ($C_4H_{10}O_7$), and 216.048 ($C_5H_{12}O_9$) for methanol and at *m/z* = 138.053 ($C_4H_{10}O_5$) for ethanol:

$$HOOCH_2OCH_2CH_3 + CH_2OO \rightleftarrows HOOCH_2OOCH_2OCH_2CH_3 \quad (R20)$$

Based on the above discussion about the isomeric composition of the $C_2H_6O_3$ signal, multiple isomeric contributions are conceivable for the higher mass intermediates in this sequence. That is, HEHP and/or MMHP could react with the CI via the insertion in the OH and/or the OOH functionality.

Reaction of the CI with aldehydes and subsequent addition reactions

The reactions of CIs with aldehydes are typically described as 1,3-dipolar cycloadditions of the carbonyl oxide to the C=O double bond of the aldehyde functional group.[80] The reaction of formaldehyde with the CI should lead to the secondary ozonide (1,2,4-trioxolane, *cycl.*-CH_2OCH_2OO-) as hypothesized by Criegee and calculated later by Jalan *et al.*[80] However, as described in Ref. [46], the detection of this intermediate was not possible under our experimental conditions and instead the ketohydroperoxide hydroperoxy acetaldehyde ($HOOCH_2CHO$) was detected. The presence of the hydroxymethylformate [$HC(=O)OCH_2OH$], an expected decomposition product of the secondary ozonide, was not unambiguously confirmed.

The reaction of acetaldehyde with the CI, which should be considered similar to the formaldehyde+CI reaction, should form a secondary ozonide; 3-methyl-1,2,4-trioxolane [*cycl.*-

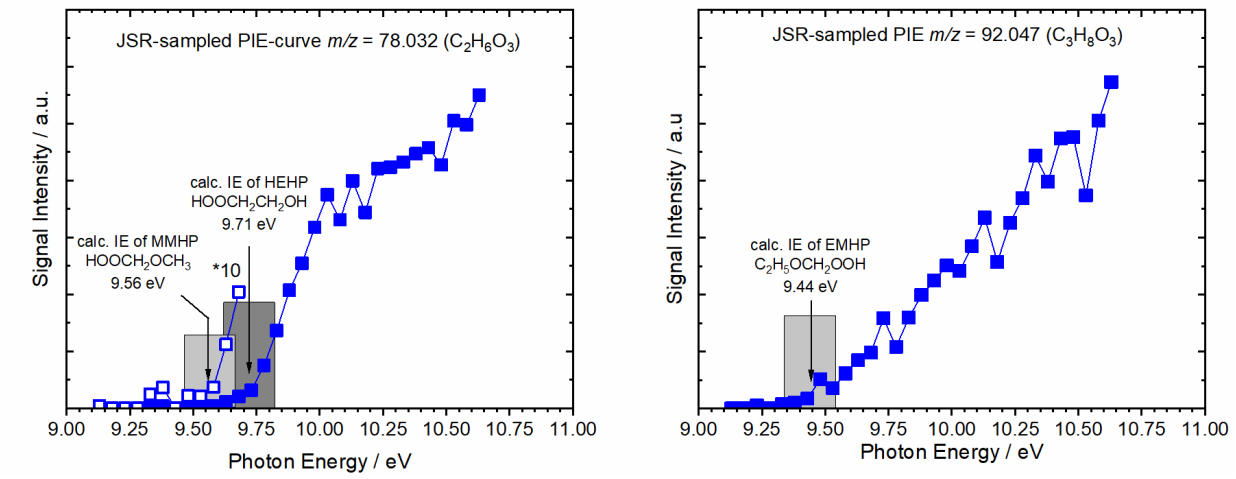

Figure 6: JSR-sampled PIE curve for (left) *m/z* = 78.032 ($C_2H_6O_3$) and (right) *m/z* = 92.047 ($C_3H_8O_3$) from the ozonolysis experiments are compared with theoretical calculations for $HOOCH_2OCH_3$ (MMHP) and $HOOCH_2CH_2OH$ (HEHP) and $HOOCH_2CH_2OH$ (EHPM), respectively.

$CH(CH_3)OCH_2OO$-]. However, Taatjes *et al.*,[30] who studied this reaction experimentally, did not detect the secondary ozonide and were only able to detect acetic acid and formaldehyde as products. The adiabatic ionization energy for this ozonide was calculated to be 9.44 eV. Jalan *et al.* have theoretically identified hydroxyethylformate [HEF, $HC(=O)OCH(OH)CH_3$] and hydroxymethylacetate [HMA, $CH_3C(=O)OCH_2OH$] as the energetically preferred intermediates of the $CH_3CHO+CH_2OO$ reaction.[80]

The experimental PIE curve for *m/z* = 90.032 ($C_3H_6O_3$), which is shown in Fig. 7, reveals a threshold for ionization near 9.62 eV. At the level of theory applied in this work, the computed IE for the secondary ozonide itself is 9.39 eV (9. 44 eV at the CBS-QB3 level[30]), which is outside the combined expected experimental and theoretical uncertainties. It should also be noted in our previous results that no primary SOZ ($C_2H_4 + O_3$) was experimentally observed, and in fact none of the identified intermediates contained cyclic structures. Therefore, it is more likely that a decomposition product is being observed instead of the SOZ itself.

Ionization energies for the HEF and HMA isomers were calculated to be 10.43 and 10.20 eV, respectively. As seen in Fig. 7, the ionization energy of the HEF is far above the observed ionization threshold and given the lack of knowledge about the individual PIE curves of the other potential isomers, no experimental evidence for the presence of HEF in the system is found. The calculated IE for HMA matches the observed feature near 10.2 eV in the experimental PIE curve, although such a feature does not necessarily indicate the presence of a new species. Furthermore, considering the predicted low-energy barrier for decomposition of HEF and HMA, the results of Jalan *et al.* [80] may indicate that HEF and HMA are not stable intermediates at the given conditions.

The observed threshold for ionization near 9.62 (±0.05) eV is consistent with the theoretically calculated 9.57 eV for the calculated IE of 1-hydroperoxypropan-2-one [$CH_3C(=O)CH_2OOH$], which appears to be an insertion product of the CI into the C-H bond from the aldehyde -C(=O)H functional group. Possible reaction pathways towards this intermediate still need to be explored.

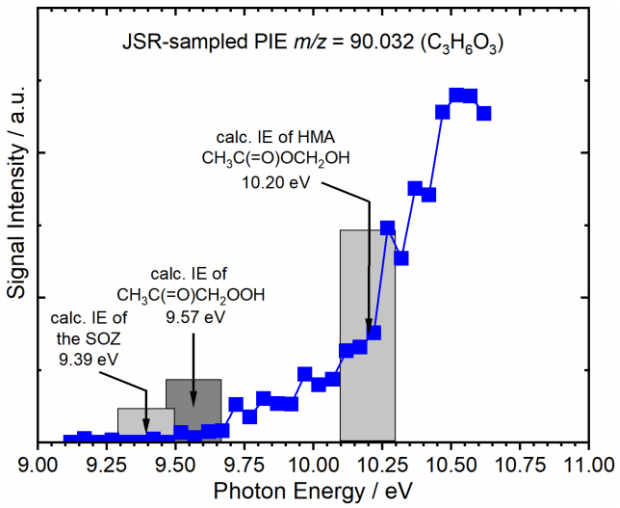

Figure 7: JSR-sampled PIE curve for *m/z* = 90.032 ($C_3H_6O_3$) after ozonolysis of ethylene. The experimental PIE curve is compared with theoretical calculations for $CH_3C(=O)CH_2OOH$, HEF, and HMA.

In this discussion, contributions from ethenol (CH_2CHOH), which had been detected in the experiments,[46] are neglected, although the CI could potentially react with the C=C double bond and the OH function of the enol.[74] While an unambiguous assignment of the isomeric structures of the $C_3H_6O_3$ intermediates is currently not feasible, it is worth noting that all of these intermediates contain a reactive -OH or -OOH group and could potentially serve as a reactant for additional CI addition reactions. And, indeed, the observation of intermediates at *m/z* = 90.032 ($C_3H_6O_3$), 136.037 ($C_4H_8O_5$), and 182.043 ($C_5H_{10}O_7$) indicates sequential addition reactions of acetaldehyde and the CI. Given the complex isomeric contributions of the $C_3H_6O_3$ intermediate, additional information of the other products concerning their isomeric structures cannot be gained.

Reaction of the CI with hydroperoxides and subsequent addition reactions

As shown in Ref. [46], small hydroperoxide species such as H_2O_2, CH_3OOH, and C_2H_5OOH were found to be present in the reactive mixture during the ozonolysis experiments. Vereecken *et al.* has shown theoretically that the CI reactions with alkyl hydroperoxides are not fast.[75] Nevertheless, hydroperoxides can react with the CI and initiate addition reactions. For example, with hydrogen peroxide:

$$H_2O_2 + CH_2OO \rightleftarrows HOOCH_2OOH \quad (R21)$$

$$HOOCH_2OOH + CH_2OO \rightleftarrows HOO(CH_2OO)_2H \quad (R22)$$

$$HOO(CH_2OO)_2H + CH_2OO \rightleftarrows HOO(CH_2OO)_3H \quad (R23)$$

These reaction intermediates were identified by their *m/z* ratio at 80.011 (CH_4O_4), 126.016 ($C_2H_6O_6$), and 172.022 ($C_3H_8O_8$). In addition, the experimentally observed PIE curve for CH_4O_4 is consistent with the calculated ionization energy of the dihydroperoxy methane (DHPM, $HOOCH_2OOH$), see Fig. 8. The calculated ionization energy of 9.89 eV is consistent with the experimentally observed ionization threshold of 9.85 eV.

The reactions of the methyl and ethyl hydroperoxides are more difficult to interpret. According to the theoretical calculations of Vereecken *et al.*,[75] the $HOOCH_2OOCH_3$ represents a deep well. However, as seen in Fig. 9, the calculated ionization energy for this compound of 9.34 eV does not match the experimentally observed threshold near 9.77 (±0.05) eV for *m/z* = 94.027 ($C_2H_6O_4$). A similar situation occurs for $C_3H_8O_4$, conceivably a product of the ethylhydroperoxide+CI reaction. Although C_2H_5OOH was identified in our earlier work,[46] the experimentally observed PIE curve for *m/z* = 108.042 ($C_3H_8O_4$) with an onset at 9.52 eV (±0.05) eV is not consistent with the $C_2H_5OOCH_2OOH$ isomer, for which an ionization energy of 9.19 eV was calculated.

According to the Vereecken *et al.* calculations,[75] the ether oxide $CH_3O(-O)CH_2OOH$ can be formed in substantial amounts in the reaction of the CI with CH_3OOH. The calculated adiabatic ionization energy for this intermediate was calculated to be 8.60 eV, substantially below the observed ionization threshold at *m/z* = 94.027 ($C_2H_6O_4$). Due to very small Franck-Condon overlaps, we may not be able to detect this intermediate near this ionization threshold.

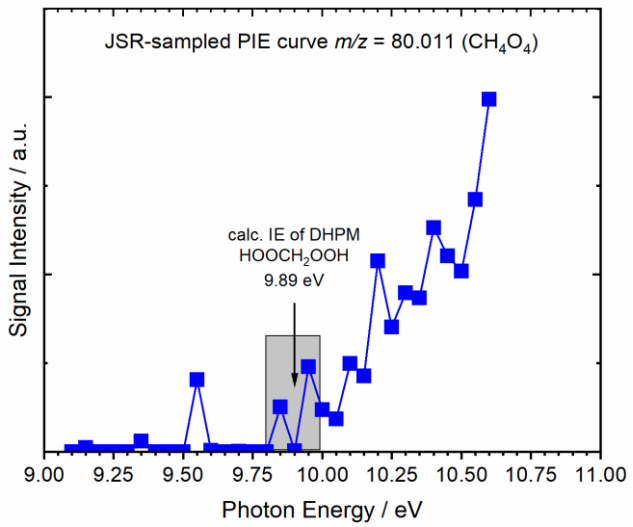

Figure 8: JSR-sampled PIE curve for *m/z* = 80.011 (CH_4O_4) after ozonolysis of ethylene. The experimental PIE curve is compared with theoretical calculations for dihydroperoxy methane (DHPM).

The calculated vertical ionization energy of 9.72 eV would match the observed threshold in the PIE curve (see. Fig. 9). However, based on the potential diagram given in Ref. [75], this species may be unstable and therefore not observable in our experiment. Similarly, the reaction of C_2H_5OOH with the CI would lead to the ether oxide $C_2H_5O(-O)CH_2OOH$, although theoretical calculations with the potential energy surface for this reaction have not been performed. The adiabatic and vertical ionization energies for this species were calculated to 8.46 and 9.55 eV, respectively. As seen in Fig. 9, the vert. IE would match the observed ionization threshold closely. As for the $CH_3O(-O)CH_2OOH$, due to strong structural changes between the ground state neutral and the ground state ion, small Franck-Condon factors are expected, which lead to experimental insensitivities near the adiabatic ionization energy. However, the agreement between the calculated vertical ionization energies and observed ionization thresholds should not be interpreted as a successful species identification. Such an assignment would require a more detailed Franck-Condon factor analysis.

Interestingly, the observed ionization onset would also be consistent with the $HOOCH_2OCH_2OH$ isomer (calc. IE of 9.66 eV). But it is not obvious how this isomer could be formed through the CI + CH_3OOH reaction. The methylhydroperoxide was clearly identified based on the PIE curve and ionization threshold and no evidence was found for the $HOCH_2OH$ isomer at *m/z* = 48.021.[46] To help interpret the experimental observations for C_3H_8O4, we also calculated the ionization energy of the $HOC_2H_4OCH_2OOH$ isomer and found an ionization energy of 9.04 eV. However, an analysis of the ion states, revealed substantial structural changes compared to the neutral, and thus, it can be argued that poor Franck-Condon overlaps results in low detection efficiency near the ionization threshold. The first locally adiabatic ionization energy with similar neutral and ion structures was calculated to be at 9.57 eV, consistent with the experimental observations (see Fig. 9).

The interpretation of the PIE curve, especially the "missing" CH_3OOCH_2OOH and $C_2H_5OOCH_2OOH$ isomers, points towards a lack of understanding of the CI+alkylhydroperoxide reactions and missing pathways in the reaction scheme.

A CI addition sequence beyond the first addition was observed for the ethylhydroperoxide but not the methylhydroperoxide. Beyond *m/z* = 108.042 ($C_3H_8O_4$), intermediates were observed at 154.048 ($C_4H_{10}O_6$) and 200.053 ($C_5H_{12}O_8$). Given the multi-functional character of the likely initial $C_3H_8O_4$ intermediate, many reaction pathways with many different intermediates become plausible. However, it is likely that these intermediates consist of long-chain hydroperoxide molecules with a CH_2OO unit.

The intensities of the ion signals, as discussed further below also reveal the low reactivity of the hydroperoxides with the CI.

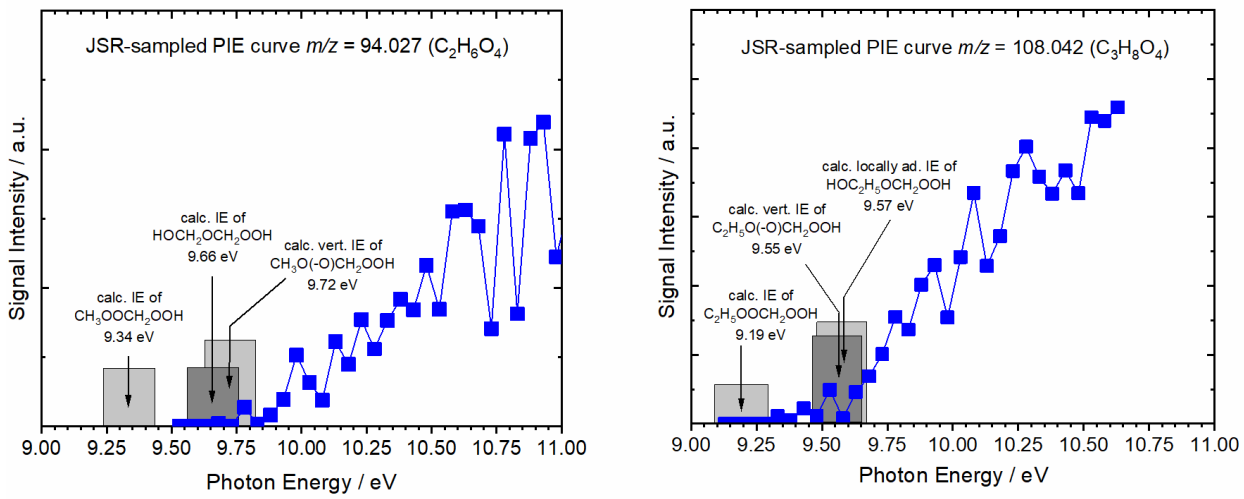

Figure 9: Left: JSR-sampled PIE curve for *m/z* = 94.027 ($C_2H_6O_4$) after ozonolysis of ethylene. The experimental PIE curve is compared with theoretical calculations for CH_3OOCH_2OOH, $HOCH_2OCH_2OOH$, and the vert. IE for $CH_3O(-O)CH_2OOH$. Right: JSR-sampled PIE curve for *m/z* = 108.042 ($C_3H_8O_4$) after ozonolysis of ethylene. The experimental PIE curve is compared with theoretical calculations for $C_2H_5OOCH_2OOH$, loc. ad. IE of $HOC_2H_5OCH_2OOH$, and the vert. IE of $C_2H_5O(-O)CH_2OOH$.

Reaction of the CI with multi-functional intermediates and subsequent addition reactions

Multi-functional intermediates are molecules that contain more than one functional group that could potentially react with the CI. For example, Rousso *et al.* have shown that hydroxy-acetaldehyde ($HOCH_2CHO$) is a common intermediate in the ozone-assisted oxidation of ethylene.[46] These molecules can react either via the OH functional group with the CI or with the aldehyde function. Another multi-functional intermediate that should be considered in this work is the hydroperoxy acetaldehyde [$HOOCH_2CHO$] that had been positively identified at *m/z* = 76.016 ($C_2H_4O_3$).[46] Similarly to the hydroxy-acetaldehyde, this intermediate has two functional groups and could react either via the insertion of the CI into the molecule's OOH group or via a cycloaddition reaction with the aldehyde group.

For the hydroxy-acetaldehyde, the 1,3-cycloaddition of the CI to the aldehyde function would lead to 1,2-dihydroxyethyl formate [$HC(=O)OCH(OH)CH_2OH$] and/or hydroxymethyl 2-hydroxyacetate [$HOCH_2C(=O)OCH_2OH$] via a secondary ozonide. The insertion of the CI to the OH group results in the formation of 2-(hydroperoxymethoxy)acetaldehyde (HPMA, $HOOCH_2OCH_2CHO$) at *m/z* = 106.027 ($C_3H_6O_4$):

$$HOCH_2CHO + CH_2OO \rightleftarrows HOOCH_2OCH_2CHO \qquad (R24)$$

The calculated IE of the HPMA isomer of 9.59 eV does not match the observed ionization onset in the PIE curve of *m/z* = 106.027, as shown in Fig. 10. However, the calculated IEs for the $HC(=O)OCH(OH)CH_2OH$ and the $HOCH_2C(=O)OCH_2OH$ isomers, 9.83 and 9.99 eV, respectively, are consistent with the observed ionization threshold. As with the acetaldehyde+CI reaction intermediate, these products cannot be unambiguously identified.

The detection of these intermediates reveals that reactions of the aldehyde function are likely faster than the insertion reactions into the hydroxy groups.

The PIE curve for *m/z* = 122.022 ($C_3H_6O_5$) is also shown in Fig. 10. It is conceivable that this intermediate is formed through a reaction of the CI with hydroperoxy-acetaldehyde ($HOOCH_2CHO$), similarly to the reactions discussed above for acetaldehyde and hydroxy-acetaldehyde. Based on the analysis in Ref [46], contributions from the hydroxymethylformate are also possible. Given the observed ionization threshold near 10.0 eV, which is similar to the one observed for the $C_3H_6O_4$ isomers, it is conceivable that the $C_3H_6O_5$ isomers also result from the 1,3-cycloaddition of the CI to the aldehyde function. But, given the size of this intermediate, we refrain from performing an analysis based on calculated ionization energies.

Additional reaction products of sequential addition reactions were observed at *m/z* = 152.032 ($C_4H_8O_6$) for the CI additions starting with the hydroxy-acetaldehyde and at *m/z* = 168.027 ($C_4H_8O_7$) and 214.032 ($C_5H_{10}O_9$) for reactions starting with the hydroperoxy-acetaldehyde.

Quantification of first step intermediates and trends in signal intensities

As described above, the mass spectral signal was converted into mole fractions (actually, $x_i \times \sigma_i$) as function of the temperature. Some representative examples for the first addition intermediate, namely CH_4O_3 (CI+H_2O), $C_2H_6O_3$ (CI+CH_3OH), $C_2H_4O_4$ (CI+HCOOH), and $C_3H_8O_3$ (CI+C_2H_5OH), can be seen in Fig. 11. For this, the data were extracted from mass spectra taken at a photon energy of 11.0 eV. Additional species traces can be found in the Supplemental Material. These species profiles follow very similar trends, which might offer some circumstantial evidence of similar formation pathways.

Analogous to the KHP and other ozonolysis species shown in Ref [46], there is monotonic decay in concentration with increasing temperature, as these highly oxygenated species decompose or are less favorable compared to smaller intermediates. By 600 K these CI created species are below the detection limit, as ozone has thermally decomposed instead of initiating ozonolysis reactions.

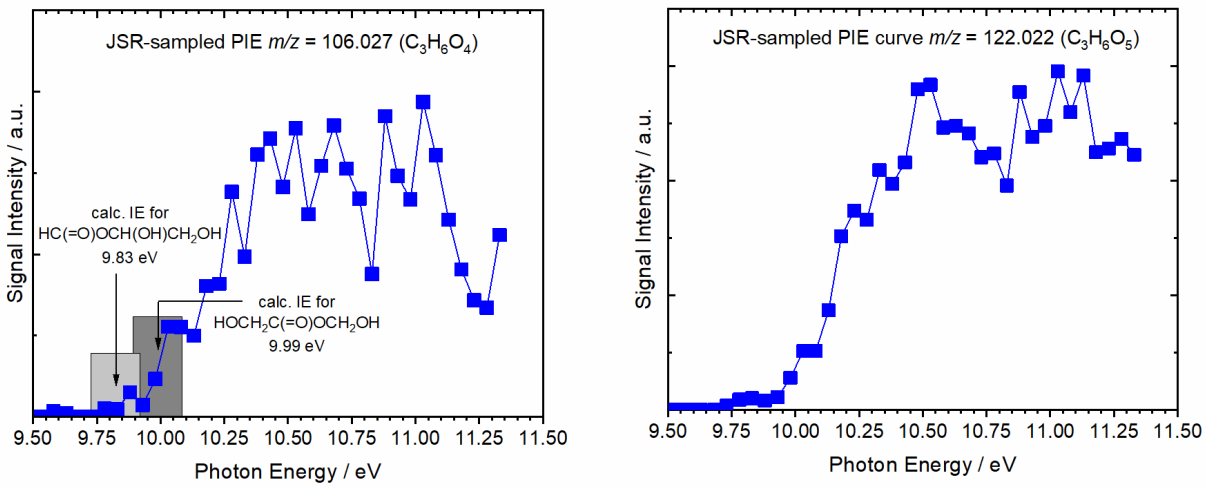

Figure 10: Left: JSR-sampled PIE curve for *m/z* = 106.027 ($C_3H_6O_4$) after ozonolysis of ethylene. The experimental PIE curve is compared with theoretical calculations for $HC(=O)OCH(OH)CH_2OH$ and $HOCH_2C(=O)OCH_2OH$. Right: JSR-sampled PIE curve for *m/z* = 122.022 ($C_3H_6O_5$) after ozonolysis of ethylene. Because of the size of this molecule, *i.e.* eight heavy atoms, we refrain from presenting an analysis based on calculated ionization energies.

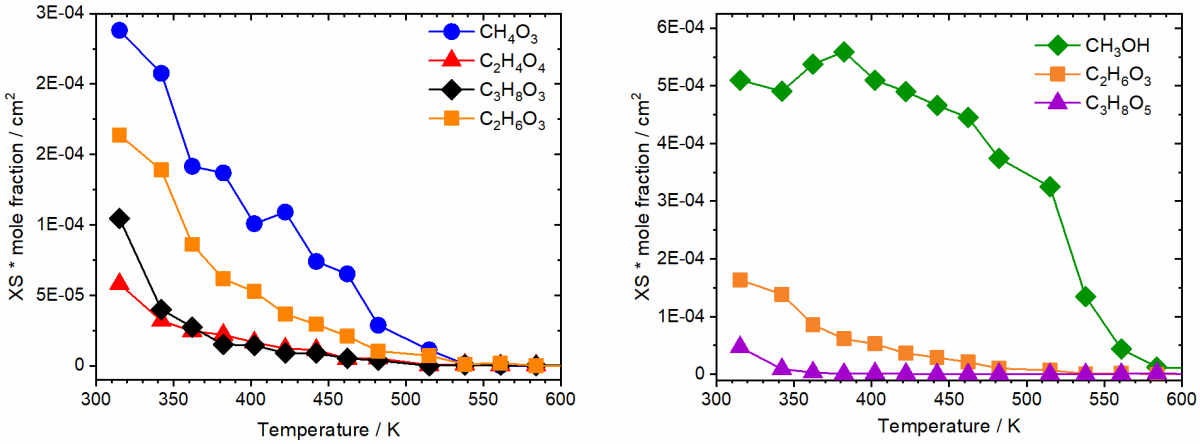

Figure 11: Mole fraction profiles as a function of temperature for the sequence of highly oxygenated species like CH_4O_3, $C_2H_4O_4$, $C_3H_8O_3$, and $C_2H_6O_3$ (left) and CH_3OH+Cl reactions (right).

In Fig. 11, HPMF ($C_2H_4O_4$) is the weakest of the species shown here, already undergoing fragmentation at this ionization energy. The CH_4O_3 concentration is likely a result of both this HPMF decomposition as well as H_2O-Cl addition, as discussed previously, as the relative cross sections are initially too weak for a signal allowing separation at lower energies. So, the CH_4O_3 signal is probably the more accurate estimate of the HPMF concentration. Methanol and ethanol both show fast Cl interactions, and therefore have strong signals for both the first, and subsequent adducts.

Many of the secondary and tertiary Cl adducts quickly fall below our detectable minimum concentration with increasing JSR temperature because the Cl is most stable at atmospheric temperature conditions or below. The signal intensities for the first Cl addition isomers, however, are strong enough for reliable temperature dependent quantification.

To illustrate the relative concentrations within a chain, the profiles for methanol (CH_3OH), first Cl addition ($C_2H_6O_3$), and second Cl addition ($C_3H_8O_5$) products are plotted in Fig. 11 as a function of temperature. While methanol is formed in significant concentration throughout the low temperature region, the Cl additions follow both the ozone and Cl trends discussed earlier: namely, monotonic decrease with increasing temperature. While the reactivity at low temperatures is at least tangentially due to ozonolysis, this suggests that methanol might have multiple formation routes besides just Cl reactions, as it does not follow the same pattern as any of the subsequent Cl adducts. There is roughly a 3x decrease in signal strength for each step in this chain. As the cross sections should be somewhat similar, this observation likely represents a significant concentration drop for each additional Cl adduct.

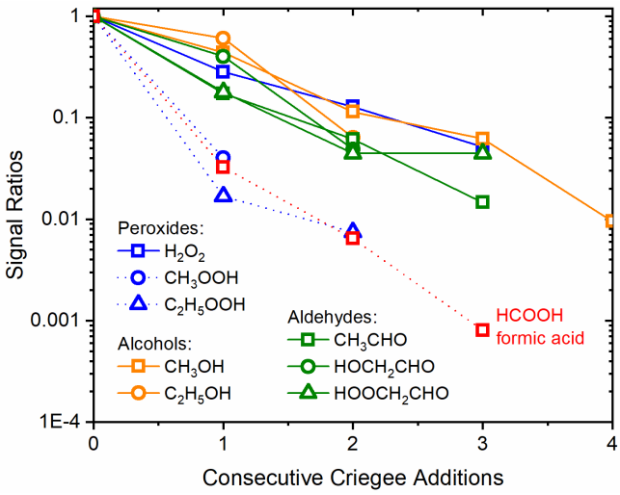

Figure 12: Signal intensities as function of number of consecutive Criegee Intermediate additions. Two slopes are identifiable with the alkylhydroperoxides reacting slower than the other intermediates.

To explore this further, the raw intensity counts can be plotted as a function of subsequent Cl additions. The ratios of signal counts on a log basis as a function of consecutive Cl additions can be seen in Fig. 12 for most of the reaction chains discussed in this paper. These counts were measured at 11eV with the exception of H_2O_2 (11.5 eV) and HCOOH (12.3eV), where 11eV is below the ionization threshold and therefore the signal artificially low. It is important to note that for various molecules, stronger or weaker signals were seen at other ionization energies, but 11eV was chosen to allow for uniform comparison and because some of the species clearly displayed fragmentation at higher energies. The zero point is the "parent" molecule in each chain, listed in the legend. The subsequent adducts have been normalized with respect to the parent molecule concentration. The hydroperoxide species, which is known from the literature to be slower and less favorable to react with Cl,[75] are seen with steeper slopes than other Cl adduct reactions. It is unclear currently why Cl + H_2O_2 seems to depart from this trend. For the second Cl adduct and beyond, we see more uniform decrease in signal counts, roughly 3-4 times weaker, which seems to largely depend on the signal strength of the first adduct. When normalized, these all seem to fall within a similar range to each other, likely demonstrating similar reaction rates. As discussed earlier, please note that there is likely significant dissociation at 11 eV, as well as contribution of HPMF to the formic acid trend, which makes the actual Cl adduct conversion rate difficult to extract. Nevertheless, this data demonstrates the highly reactive nature of the Cl with most species and confirms the slower reaction rates seen in the literature for most peroxide intermediates.

Conclusions

This study characterized the network of Criegee Intermediate reactions leading to the significant molecular growth during ethylene ozonolysis using a jet-stirred reactor and photoionization molecular beam mass spectrometry. Building off the previous work highlighting the main species in both the ozonolysis and high temperature regimes,[46] this work focused on identifying highly oxygenated species that reportedly have been found in atmospheric secondary organic aerosols. Notably, the majority of the observed mass spectra and photoionization curves associated with these species is consistent with their formation via successive CI addition reactions to typical small-molecule species. Series of species resulting from CI additions to ethylene, water, formic acid, acetaldehyde, and various alcohol and hydroperoxide species were identified. However, there seems to be a gap in our understanding of the alkylhydroperoxide + CI chemistry. The network of CI reactions identified in this paper is visualized in Fig. 13. Reaction sequences were started by reactions of the CI with C_2H_4, H_2O, HCOOH, H_2O_2, CH_3OH, C_2H_5OH, CH_3OOH, C_2H_5OOH, CH_3CHO, $HOCH_2CHO$, $HOOCH_2CHO$. Given the fact that the initial concentrations in these idealized laboratory-scale experiments are high compared to atmospheric conditions, the relevance of these pathways in real-world environments needs to be tested in future work. Nevertheless, the current study helps to understand the initial steps to the CI reaction series and provide useful context to help explain real world data.

Ozone is one of the major products in non-equilibrium plasma assisted combustion such as in the corona and microwave discharges for fuel lean HCCI ignition enhancement. Previous studies only focused on the ignition enhancement by O atom production from ozone decomposition. The present data provide another low temperature combustion enhancement pathway of ozone via ozonolysis. The present data substantially increases our knowledge about the formation of highly reactive oxygenated species via ozonolysis and its impact on low temperature fuel oxidation under fuel lean HCCI compression ignition conditions. As shown in Ref. [46], the modelling approaches of these processes are at their infancy and new validation targets, in the form of species identification and quantification are considered as useful in combination with the identification of reaction pathways. Eventually, this work can result in reactivity-controlled designs for reliable ignition statistics. In these cases, both the fuel and ozone concentrations could be quite high, leading to significant CI involvement in the initiation of LTC oxidation.

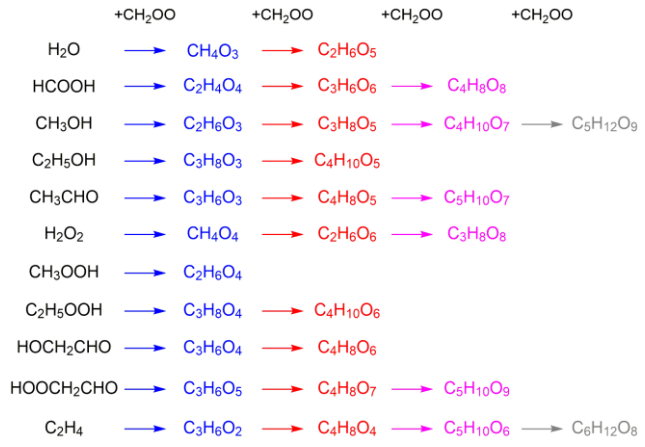

Figure 13: Network of Criegee Intermediate reactions as observed in the ozonolysis experiments of this work. The observed mass spectra are best described as originating from consecutive addition reactions of multiple CI insertion reactions with various starting molecules which are present in the gas mixture as either intermediate or product of the ozonolysis reaction system.

The observation of molecular structures at larger masses, suggests evidence for second and third CI addition to smaller species, providing experimentally based motivation for future theoretical calculations and modeling efforts aimed at quantifying the importance of the CI reaction pathways as well as the ethylene ozonolysis chemical reaction mechanism at large. The isomeric composition of the second addition reaction products still needs to be determined experimentally for gaining a more accurate understanding about the formation routes of larger molecules and possible SOA.

Conflicts of interest

There are no conflicts to declare.

Acknowledgements

ACR and YJ are grateful to the U.S. Department of Defense for their funding through the National Defense Science & Engineering Graduate (NDSEG) Fellowship program, NSF grant CBET-1507358, and Princeton SEAS innovation fund and ACEE grant. This work is supported by the U.S. Department of Energy (DOE), Office of Science, Office of Workforce Development for Teachers and Scientists, Office of Science Graduate Student Research (SCGSR) program, administered by the Oak Ridge Institute for Science and Education for the DOE under contract number DE-SC0014664. NH and AWJ acknowledge support from the U.S. DOE, Office of Science, Office of Basic Energy Sciences. We gratefully acknowledge computing resources provided by Bebop, a high-performance computing cluster operated by the Laboratory Computing Resource Center at Argonne National Laboratory. Sandia National Laboratories is a multi-mission laboratory managed and operated by National Technology and Engineering Solutions of Sandia, LLC., a wholly owned subsidiary of Honeywell International, Inc., for the U.S. DOE National Nuclear Security Administration under contract DE-NA0003525. AWJ is supported by the Division of Chemical Sciences, Geosciences, and Biosciences, under Contract Number DE-AC02-06CH11357. The Advanced Light Source is supported by the Director, Office of Science, Office of Basic Energy Sciences, of the U.S. DOE under Contract No. DEAC02-05CH11231. The authors gratefully acknowledge Paul Fugazzi for technical assistance and Stephen Klippenstein (Argonne National Laboratory) for helpful discussions.

Notes and references

1 R. Criegee and G. Wenner, *Liebigs Ann. Chem.*, 1949, **564**, 9-15.
2 R. Criegee, *Angew. Chem. Int. Ed.*, 1975, **14**, 745-752.

3 L. Vereecken and J. S. Francisco, *Chem. Soc. Rev.*, 2012, **41**, 6259-6293.
4 J. Anglada, J. Gonzalez and M. Torrent-Sucarrat, *Phys. Chem. Chem. Phys.*, 2011, **13**, 13034-13045.
5 E. Miliordos and S. S. Xantheas, *Angew. Chem. Int. Ed.*, 2016, **55**, 1015-1019.
6 L. Vereecken, A. Novelli and D. Taraborrelli, *Phys. Chem. Chem. Phys.*, 2017, **19**, 31599-31612.
7 M. J. Newland, A. R. Rickard, L. Vereecken, A. Muñoz, M. Ródenas and W. J. Bloss, *J. Atmos. Chem. Phys.*, 2015, **15**, 9521-9536.
8 R. Atkinson and J. Arey, *Chem. Rev.*, 2003, **103**, 4605-4638.
9 J. Ahrens, P. T. Carlsson, N. Hertl, M. Olzmann, M. Pfeifle, J. L. Wolf and T. Zeuch, *Angew. Chem. Int. Ed.*, 2014, **53**, 715-719.
10 L. Vereecken, H. Harder and A. Novelli, *Phys. Chem. Chem. Phys.*, 2012, **14**, 14682-14695.
11 R. L. Caravan, M. A. H. Khan, B. Rotavera, E. Papajak, I. O. Antonov, M.-W. Chen, K. Au, W. Chao, D. L. Osborn, J. J.-M. Lin, C. J. Percival, D. E. Shallcross and C. A. Taatjes, *Faraday Disc.*, 2017, **200**, 313-330.
12 M. J. Newland, A. R. Rickard, M. S. Alam, L. Vereecken, A. Muñoz, M. Ródenas and W. J. Bloss, *Phys. Chem. Chem. Phys.*, 2015, **17**, 4076-4088.
13 D. Stone, M. Blitz, L. Daubney, N. U. M. Howes and P. Seakins, *Phys. Chem. Chem. Phys.*, 2014, **16**, 1139-1149.
14 R. Chhantyal-Pun, A. Davey, D. E. Shallcross, C. J. Percival and A. J. Orr-Ewing, *Phys. Chem. Chem. Phys.*, 2015, **17**, 3617-3626.
15 A. S. Hasson, M. Y. Chung, K. T. Kuwata, A. D. Converse, D. Krohn and S. E. Paulson, *J. Phys. Chem. A*, 2003, **107**, 6176-6182.
16 A. A. Presto and N. M. Donahue, *J. Phys. Chem. A*, 2004, **108**, 9096-9104.
17 Y. Sakamoto, S. Inomata and J. Hirokawa, *J. Phys. Chem. A*, 2013, **117**, 12912-12921.
18 M. Ehn, J. A. Thornton, E. Kleist, M. Sipilä, H. Junninen, I. Pullinen, M. Springer, F. Rubach, R. Tillmann and B. Lee, *Nature*, 2014, **506**, 476.
19 A. A. Presto, K. E. Huff Hartz and N. M. Donahue, *J. Environ. Sci. Tech.*, 2005, **39**, 7046-7054.
20 S. Gao, M. Keywood, N. L. Ng, J. Surratt, V. Varutbangkul, R. Bahreini, R. C. Flagan and J. H. Seinfeld, *J. Phys. Chem. A*, 2004, **108**, 10147-10164.
21 P. J. Ziemann and R. Atkinson, *Chem. Soc. Rev.*, 2012, **41**, 6582-6605.
22 B. Yang, P. Ma, J. Shu, P. Zhang, J. Huang and H. Zhang, *Environ. Poll.*, 2018, **234**, 960-968.
23 D. L. Osborn and C. A. Taatjes, *Int. Rev. Phys. Chem.*, 2015, **34**, 309-360.
24 C. A. Taatjes, *Annu. Rev. Phys. Chem.*, 2017, **68**, 183-207.
25 P. Neeb, O. Horie and G. K. Moortgat, *J. Phys. Chem. A*, 1998, **102**, 6778-6785.
26 P. Neeb, H. Osamu and G. K. Moortgat, *Int. J. Chem. Kin.*, 1996, **28**, 721-730.
27 P. Neeb, F. Sauer, O. Horie and G. K. Moortgat, *Atmos. Environ.*, 1997, **31**, 1417-1423.
28 O. Welz, J. D. Savee, D. L. Osborn, S. S. Vasu, C. J. Percival, D. E. Shallcross and C. A. Taatjes, *Science*, 2012, **335**, 204-207.
29 Z. J. Buras, R. M. I. Elsamra, A. Jalan, J. E. Middaugh and W. H. Green, *J. Phys. Chem. A*, 2014, **118**, 1997-2006.
30 C. A. Taatjes, O. Welz, A. J. Eskola, J. D. Savee, D. L. Osborn, E. P. F. Lee, J. M. Dyke, D. W. K. Mok, D. E. Shallcross and C. J. Percival, *Phys. Chem. Chem. Phys.*, 2012, **14**, 10391-10400.
31 M. Olzmann, E. Kraka, D. Cremer, R. Gutbrod and S. Andersson, *J. Phys. Chem. A*, 1997, **101**, 9421-9429.
32 T. L. Nguyen, H. Lee, D. A. Matthews, M. C. McCarthy and J. F. Stanton, *J. Phys. Chem. A*, 2015, **119**, 5524-5533.
33 A. B. Ryzhkov and P. A. Ariya, *Phys. Chem. Chem. Phys.*, 2004, **6**, 5042-5050.
34 O. B. Gadzhiev, S. K. Ignatov, B. E. Krisyuk, A. V. Maiorov, S. Gangopadhyay and A. E. Masunov, *J. Phys. Chem. A*, 2012, **116**, 10420-10434.
35 N. I. Watson, J. A. Black, T. M. Stonelake, P. J. Knowles and J. M. Beames, *J. Phys. Chem. A*, 2018, **DOI: 10.1021/acs.jpca.8b09349**.
36 L. Vereecken, H. Harder and A. Novelli, *Phys. Chem. Chem. Phys.*, 2014, **16**, 4039-4049.
37 Y. Sakamoto, R. Yajima, S. Inomata and J. Hirokawa, *Phys. Chem. Chem. Phys.*, 2017, **19**, 3165-3175.
38 M. L. Walser, Y. Desyaterik, J. Laskin, A. Laskin and S. A. Nizkorodov, *Phys. Chem. Chem. Phys.*, 2008, **10**, 1009-1022.
39 M. Hallquist, J. C. Wenger, U. Baltensperger, Y. Rudich, D. Simpson, M. Claeys, J. Dommen, N. Donahue, C. George and A. Goldstein, *J. Atmos. Chem. Phys.*, 2009, **9**, 5155-5236.
40 Y. Ju and W. Sun, *Progr. Energy Combust. Sci.*, 2015, **48**, 21-83.
41 X. Gao, J. Zhai, W. Sun, T. Ombrello and C. D. Carter, in *54th AIAA Aerospace Sciences Meeting*, American Institute of Aeronautics and Astronautics, 2016.
42 X. Gao, Y. Zhang, S. Adusumilli, J. Seitzman, W. Sun, T. Ombrello and C. Carter, *Combust. Flame*, 2015, **162**, 3914-3924.
43 T. Nomaguchi and S. Koda, *Proc. Combust. Inst.*, 1989, **22**, 1677-1682.
44 T. Ombrello, S. H. Won, Y. Ju and S. Williams, *Combust. Flame*, 2010, **157**, 1906-1915.
45 H. Zhao, X. Yang and Y. Ju, *Combust. Flame*, 2016, **173**, 187-194.
46 A. C. Rousso, N. Hansen, A. W. Jasper and Y. Ju, *J. Phys. Chem. A*, 2018, **122**, 8674-8685.
47 K. Hoyermann, F. Mauß, M. Olzmann, O. Welz and T. Zeuch, *Phys. Chem. Chem. Phys.*, 2017, **19**, 18128-18146.
48 M. P. Tolocka, M. Jang, J. M. Ginter, F. J. Cox, R. M. Kamens and M. V. Johnston, *Environ. Sci. Tech.*, 2004, **38**, 1428-1434.
49 L. Chen, Y. Huang, Y. Xue, J. Cao and W. Wang, *Atmos. Environ.*, 2018, **187**, 218-229.
50 Q. Zhao, W. Wang, F. Liu, J. Lü and W. Wang, *Atmos. Environ.*, 2017, **166**, 1-8.
51 K. Moshammer, A. W. Jasper, D. M. Popolan-Vaida, A. Lucassen, P. Diévart, H. Selim, A. J. Eskola, C. A. Taatjes, S. R. Leone, S. M. Sarathy, Y. Ju, P. Dagaut, K. Kohse-Höinghaus and N. Hansen, *J. Phys. Chem. A*, 2015, **119**, 7361-7374.
52 K. Moshammer, A. W. Jasper, D. M. Popolan-Vaida, Z. Wang, V. S. Bhavani Shankar, L. Ruwe, C. A. Taatjes, P. Dagaut and N. Hansen, *J. Phys. Chem. A*, 2016, **120**, 7890-7901.
53 J. Orphal, J. Staehelin, J. Tamminen, G. Braathen, M.-R. De Backer, A. Bais, D. Balis, A. Barbe, P. K. Bhartia, M. Birk, J. B. Burkholder, K. Chance, T. von Clarmann, A. Cox, D. Degenstein, R. Evans, J.-M. Flaud, D. Flittner, S. Godin-Beekmann, V. Gorshelev, A. Gratien, E. Hare, C. Janssen, E. Kyrölä, T. McElroy, R. McPeters, M. Pastel, M. Petersen, I. Petropavlovskikh, B. Picquet-Varrault, M. Pitts, G. Labow, M. Rotger-Languereau, T. Leblanc, C. Lerot, X. Liu, P. Moussay, A. Redondas, M. Van Roozendael, S. P. Sander, M. Schneider, A. Serdyuchenko, P. Veefkind, J. Viallon, C. Viatte, G. Wagner, M. Weber, R. I. Wielgosz and C. Zehner, *J. Mol. Spectrosc.*, 2016, **327**, 105-121.
54 W. Sun, T. Tao, M. Lailliau, N. Hansen, B. Yang and P. Dagaut, *Combust. Flame*, 2018, **193**, 491-501.

55 T. Tao, W. Sun, N. Hansen, A. W. Jasper, K. Moshammer, B. Chen, Z. Wang, C. Huang, P. Dagaut and B. Yang, *Combust. flame*, 2018, **192**, 120-129.
56 F. N. Egolfopoulos, N. Hansen, Y. Ju, K. Kohse-Höinghaus, C. K. Law and F. Qi, *Progr. Energy Combust. Sci.*, 2014, **43**, 36-67.
57 N. Hansen, T. A. Cool, P. R. Westmoreland and K. Kohse-Höinghaus, *Progr. Energy Combust. Sci.*, 2009, **35**, 168-191.
58 S. R. Leone, M. Ahmed and K. R. Wilson, *Phys. Chem. Chem. Phys.*, 2010, **12**, 6564-6578.
59 T. A. Cool, K. Nakajima, C. A. Taatjes, A. McIlroy, P. R. Westmoreland, M. E. Law and A. Morel, *Proc. Combust. Inst.*, 2005, **30**, 1681-1688.
60 N. Hansen, S. J. Klippenstein, J. A. Miller, J. Wang, T. A. Cool, M. E. Law, P. R. Westmoreland, T. Kasper and K. Kohse-Höinghaus, *J. Phys. Chem. A*, 2006, **110**, 4376-4388.
61 N. Hansen, S. J. Klippenstein, C. A. Taatjes, J. A. Miller, J. Wang, T. A. Cool, B. Yang, R. Yang, L. Wei and C. Huang, *J. Phys. Chem. A*, 2006, **110**, 3670-3678.
62 N. Hansen, S. J. Klippenstein, P. R. Westmoreland, T. Kasper, K. Kohse-Höinghaus, J. Wang and T. Cool, *Phys. Chem. Chem. Phys.*, 2008, **10**, 366-374.
63 N. Hansen, T. Kasper, S. J. Klippenstein, P. R. Westmoreland, M. E. Law, C. A. Taatjes, K. Kohse-Höinghaus, J. Wang and T. A. Cool, *J. Phys. Chem. A*, 2007, **111**, 4081-4092.
64 C. A. Taatjes, N. Hansen, D. L. Osborn, K. Kohse-Höinghaus, T. A. Cool and P. R. Westmoreland, *Phys. Chem. Chem. Phys.*, 2008, **10**, 20-34.
65 F. Qi, *Proc. Combust. Inst.*, 2013, **34**, 33-63.
66 N. M. O'Boyle, M. Banck, C. A. James, C. Morley, T. Vandermeersch and G. R. Hutchison, *J. Cheminformatics*, 2011, **3**, 33.
67 The Open Babel Package, Version 2.3.1., http://openbabel.org, (accessed accessed Oct. 2011).
68 P. R. Story and J. R. Burgess, *J. Am. Chem. Soc.*, 1967, **89**, 5726-5727.
69 R. Crehuet, J. M. Anglada, D. Cremer and J. M. Bofill, *J. Phys. Chem. A*, 2002, **106**, 3917-3929.
70 Y. Lan, L. Zou, Y. Cao and K. N. Houk, *J. Phys. Chem. A*, 2011, **115**, 13906-13920.
71 M. Pfeifle, Y.-T. Ma, A. W. Jasper, L. B. Harding, W. L. Hase and S. J. Klippenstein, *J. Chem. Phys.*, 2018, **148**, 174306.
72 A. Rodriguez, O. Herbinet, Z. Wang, F. Qi, C. Fittschen, P. R. Westmoreland and F. Battin-Leclerc, *Proc. Combust. Inst.*, 2017, **36**, 333-342.
73 A. Rodriguez, O. Herbinet, X. Meng, C. Fittschen, Z. Wang, L. Xing, L. Zhang and F. Battin-Leclerc, *J. Phys. Chem. A*, 2017, **121**, 1861-1876.
74 L. Vereecken, *Phys. Chem. Chem. Phys.*, 2017, **19**, 28630-28640.
75 L. Vereecken, A. Rickard, M. Newland and W. Bloss, *Phys. Chem. Chem. Phys.*, 2015, **17**, 23847-23858.
76 S. V. Tadayon, E. S. Foreman and C. Murray, *J. Phys. Chem. A*, 2017, **122**, 258-268.
77 A. S. Hasson, G. Orzechowska and S. E. Paulson, *J. Geophys. Res. Atmos.*, 2001, **106**, 34131-34142.
78 R. Crehuet, J. M. Anglada and J. M. Bofill, *Chem. Euro. J.*, 2001, **7**, 2227-2235.
79 L.-C. Lin, H.-T. Chang, C.-H. Chang, W. Chao, M. C. Smith, C.-H. Chang and K. Takahashi, *Phys. Chem. Chem. Phys.*, 2016, **18**, 4557-4568.
80 A. Jalan, J. W. Allen and W. H. Green, *Phys. Chem. Chem. Phys.*, 2013, **15**, 16841-16852.

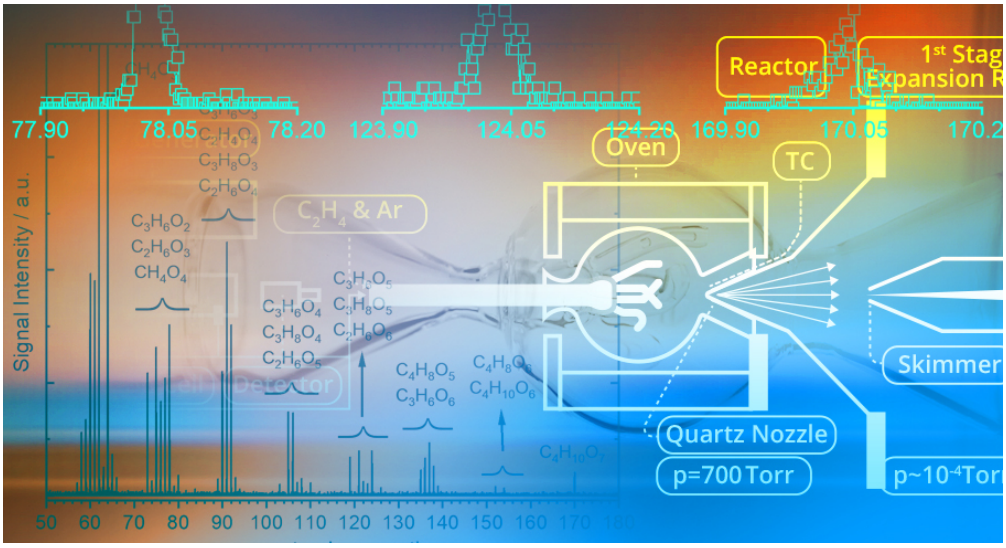

319x172mm (72 x 72 DPI)